DTU Library

Potassium Capture by Kaolin, Part 1: KOH

Wang, Guoliang; Jensen, Peter Arendt; Wu, Hao; Jappe Frandsen, Flemming; Sander, Bo; Glarborg, Peter

Potassium-capture by Kaolin. Part 1: KOH

Guoliang Wang[†], Peter Arendt Jensen[†], Hao Wu[†], Flemming Jappe Frandsen[†], Bo Sander[††], Peter Glarborg[†]*

[†]Department of Chemical and Biochemical Engineering, Technical University of Denmark, Søltofts Plads, Building 229, DK-2800 Kgs. Lyngby, Denmark

[††]Ørsted Bioenergy & Thermal Power A/S, Kraftværksvej 53, 7000 Fredericia, Denmark

*Corresponding author email-id: guow@kt.dtu.dk

Abstract: The reaction of gaseous KOH with kaolin and mullite powder at suspension-fired conditions was studied by entrained flow reactor (EFR) experiments. A water based slurry containing kaolin/mullite and KOH was fed into the reactor and the reacted solid samples were analyzed to quantify the K-capture level. The effect of reaction temperature, K-concentration in the flue gas and thereby molar ratio of K/(Al+Si) in reactants, gas residence time, and solid particle size on K-capture reaction was systematically investigated. Corresponding equilibrium calculations were conducted with FactSage 7.0. The experimental results showed that kaolin reached almost full conversion to K-aluminosilicates at suspension-fired conditions at 1100 - 1450 °C for a residence time of 1.2 s and a particle size of D_{50} = 5.47 μm. The amount of potassium captured by kaolin generally followed the equilibrium at temperatures above 1100 °C, but lower conversion was observed at 800 °C and 900 °C.

1

Crystalline kaliophilite ($KAlSiO_4$) was formed at higher temperatures (1300 °C and 1450 °C), whereas, amorphous K-aluminosilicate was formed at lower temperatures. Coarse kaolin (D_{50} = 13.48 μm) captured KOH less effectively than normal (D_{50} = 5.47 μm) and fine (D_{50} = 3.51 μm) kaolin powder at 1100 °C and 1300 °C. The difference was less significant at 900 °C. Mullite generated from kaolin captured KOH less effectively than kaolin at temperatures below 1100 °C. However, at 1300 °C and 1450 °C, the amount of potassium captured by mullite became comparatively to that of kaolin.

1　Introduction

Suspension-combustion boilers (also called pulverized fuel combustion boilers) are increasingly used for production of power and heat from biomass.[1, 2] Combustion of biomass in suspension-fired boilers can produce renewable, CO_2-neutral electricity with a higher electrical efficiency compared with that of grate-fired boilers.[3] However, during the combustion process of biomass, significant amounts of K-species, such as KOH, KCl and K_2SO_4, are released to gas phase in the boiler chamber, and this leads to deposit formation, corrosion [4-12] as well as de-activation of SCR (Selective Catalytic Reduction) catalysts.[13-18] Ash deposition and corrosion problems may be mitigated by reducing the super heater temperature. However, this will cause a reduced electrical efficiency of power plants.[3, 19-22]

To minimize the ash related problems in biomass combustion, different treatments and processing technologies have been developed, including use of alkali scavenging additives,[23-30] co-combustion with other biofuels or fossil fuels that are rich in Si or Al,[31-35] utilizing effective deposit removal techniques,[36] and a combination of different thermo-chemical processes.[37, 38] Among these, using additives is a promising option, primarily due to its high effectiveness and low requirements for boiler.

The basic principle of additive use is that the additives are injected to boilers to react with the problematic gaseous K-salts (such as KOH and KCl), forming K-species (such as K-aluminosilicates) with low corrosivity and high melting temperatures.[2, 23, 26, 27, 29, 39-46] Biomass firing additives can generally be categorized into Al-Si based, S-based, P-based and Ca-based, according to the major elements present in the additives.[2, 42, 47-50]

Kaolin[51-55] and coal fly ash[52] are typical Al-Si based additives for biomass combustion and have been studied in laboratory-scale experiments. In addition, coal fly ash has been utilized in full-scale biomass suspension-firing boilers in Denmark, and has been shown to have the capacity to significantly remedy deposition and corrosion problems.[29, 40] The mineralogical composition of coal fly ash is complex; including mainly mineral phases such as quartz, mullite, kaolinite, illite, siderite, etc.[56, 57] Among these mineral phases, kaolinite has been shown to be one of the most effective one for K-capture.[58] Kaolinite is a layered aluminosilicate mineral with chemical formula of $Al_2Si_2O_5(OH)_4$. Kaolin is a kind of clay that is rich in kaolinite. Investigating the K-capture reaction by kaolin is important for obtaining an improved understanding of K-capture by coal fly ash.

Kaolin undergoes complex transformation when being heated up. Above 450 °C, kaolin transfers into metakaolin via a dehydroxylation reaction as shown in reaction R1.[51] Metakaolin is a type of amorphous aluminosilicate that reacts effectively with gaseous K-salts.[51] Metakaolin further transforms into spinel structure and amorphous SiO_2 when it is heated to above 980 °C, see reaction R2. Mullite starts to form at around 1100 °C, and its amount increases with temperature and time, according to reaction R3.[59] At temperatures above 1400 °C, needle shaped mullite grains are formed, and the size and the aspect ratio of the mullite grains increase with increasing calcination temperature.[59] Generally, compared to metakaolin, mullite is believed to be less reactive for alkali capture.[52] Thus the
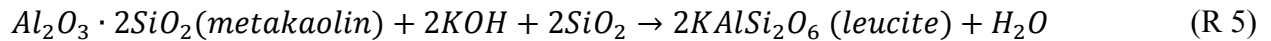
3

transformation of kaolin at high temperatures may influence the K-capture reaction. To achieve the best K-capture results, kaolin should be injected into boilers at an optimal temperature window.

$$Al_2Si_2O_5(OH)_4 \ (kaolin) \rightarrow Al_2O_3 \cdot 2SiO_2 \ (metakaolin) + 2H_2O \ (g) \qquad \text{(R 1)}$$

$$Al_2O_3 \cdot 2SiO_2 (metakaolin) \rightarrow Al_2O_3 \cdot SiO_2 \ (spinel) + SiO_2(amorphous) \qquad \text{(R 2)}$$

$$3 \ (Al_2O_3 \cdot SiO_2) \ (spinel) + 3 \ SiO_2(amorphous) \rightarrow 3Al_2O_3 \cdot 2SiO_2 \ (mullite)$$
$$+ \ 4 \ SiO_2(amorphous) \qquad \text{(R 3)}$$
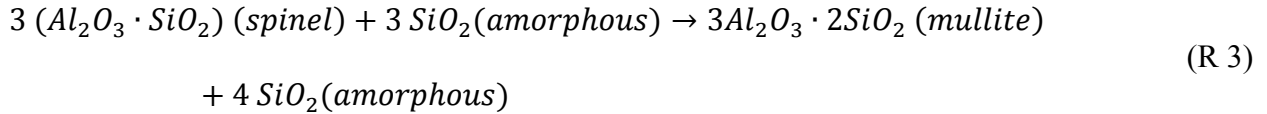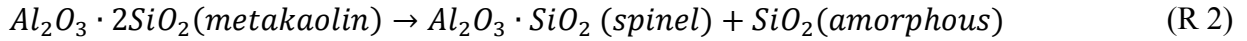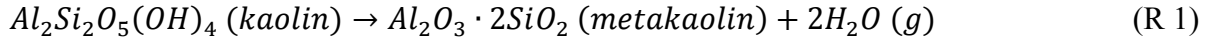
Alkali-capture, especially the Na-capture reaction by kaolin has been widely studied primarily due to its application for cleaning Na-species from hot flue gases in Combined Cycle Gas Turbine (CCGT) power plants[60-62] and for dealing with ash-related problems in combustion of Na-rich low rank coals in power plant boilers.[28, 63-66] However, when it comes to biomass combustion, K-capture reaction is of greater concern, but it has been studied to a less extent.[51]

Gas phase release and speciation of potassium depends on many factors including combustion conditions, fuel ash transformation chemistry, etc. In the combustion of biomass with high K but low Cl and S contents, KOH(g) is the dominant K-species in the high temperature flue gas.[67, 68] When S and Cl are available, KCl and K_2SO_4 would be formed during the combustion process, but at high temperature KCl and K_2SO_4 can also transfer into KOH in the presence of water.[51]

KOH is a troublesome K-species and the main reactions involved for kaolin/metakaolin to capture KOH are shown in reaction R4 and R5.[67] The two main products are kalsilite ($KAlSiO_4$) and leucite ($KAlSi_2O_6$) with melting temperatures above 1600 °C and 1500 °C, respectively. Therefore, the melt-induced slagging and corrosion in biomass-fired boilers could be significantly mitigated by the use of kaolin.[3, 22, 69] However, the kinetics and detailed knowledge on the KOH-capture reaction by kaolin is still limited, especially, for suspension combustion.

4

$$Al_2O_3 \cdot 2SiO_2(metakaolin) + 2KOH \rightarrow 2KAlSiO_4 \ (kalsilite) + H_2O \qquad \text{(R 4)}$$

$$Al_2O_3 \cdot 2SiO_2(metakaolin) + 2KOH + 2SiO_2 \rightarrow 2KAlSi_2O_6 \ (leucite) + H_2O \qquad \text{(R 5)}$$

To the author's knowledge, the only literature available on alkali-capture by dispersed kaolin particles at suspension-fired conditions is the experimental study by Wendt and co-authors[63, 70, 71] done in a 17-kW down-flow combustor which simulated the conditions in suspension-fired boilers. A sodium acetate solution was injected in the reactor to produce a Na vapor. The effect of temperature, residence time as well as the presence of sulfur and chlorine on the Na-capture reaction was studied. Results showed that the rate of NaOH adsorption was higher than that of NaCl, and they proposed that NaOH is the only reacting species in both cases. However, whether the kinetics of Na and K capture by kaolin are the same has not been established.[52]

Gaseous KOH capture by kaolin pellets (around 1 mm) in a fixed bed was studied by Steenari and co-workers.[51, 72, 73] They found that kaolin captured KCl more effectively than KOH, indicating that KCl and KOH can both react directly with kaolin. The KOH concentration was very low in these studies, with a typical KOH-concentration of 1.1 ppm, which is far below the K-concentration in biomass suspension-fired boilers.[5]

The degree of conversion of kaolin to K-aluminosilicates may be limited by equilibrium constrains. In addition, the rate of reaction may be limited by the external and internal diffusion of the gaseous potassium species, and by the reaction kinetics. Typically, a decreased kaolin particle size and/or an increased residence time lead to an increased conversion to the products.

At suspension-fired conditions, the reaction between gaseous KOH and dispersed kaolin particles may be affected by the local temperature, the additive particle size and composition, and the reaction time. Understanding the influence of different parameters on the K-capture reaction is crucial and

helpful for providing recommendation for optimal utilization of kaolin and coal fly ash in full-scale boilers.

The objective of this work is to develop a method to study the K-capture reactions by solid additives at well-controlled suspension-fired conditions, and to systematically investigate the impact of different parameters on the K-capture reaction by solid additives, such as reaction temperature, K-concentration/molar ratio of K/(Al+Si) in the reactant, kaolin particle size, gas residence time and the high temperature transformation of kaolin. This paper is Part 1 of a series of two papers studying the potassium capture by kaolin. This paper focuses on the KOH capture by kaolin, and the second one focuses on the K-capture reaction by kaolin using KCl, K_2CO_3 and K_2SO_4.

2   Experimental section

2.1 Materials

Kaolin powders of three different particle sizes and a mullite powder were utilized in this study. The particle size distribution (PSD) of the materials was analyzed with a Malvern 3000 particle size distribution analyzer. Based on the PSD, the three kaolin powders are named as normal kaolin powder (D_{50} = 5.47 μm), fine kaolin powder (D_{50} = 3.51 μm), and coarse kaolin powder (D_{50} = 13.48 μm). The normal kaolin powder was purchased from VWR Chemicals, and the fine kaolin powder was generated by grinding the normal kaolin powder in a ball mill. The coarse kaolin powder was obtained by grinding kaolin stones purchased from Ward's Science. Mullite powder was generated by heat treatment of the normal kaolin powder (D_{50} = 5.47 μm) at 1100 °C for 24 hours.[59] The calcinated mullite sample was re-grinded, to break the agglomerated blocks, and to get a D_{50} of 5.90 μm, which is similar to that of the normal kaolin powder (D_{50} = 5.47 μm).

The materials were analyzed by ICP-OES (Inductively Coupled Plasma Atomic Emission Spectroscopy) and XRD (X-ray Diffraction), for elemental composition and mineralogical composition. The elemental composition of the three kaolin samples was similar, as shown in Table 1. The molar (Na + K)/(Si + Al) ratio of the three kaolin samples is around 0.02, indicating that a large fraction of Al and Si are available for K-capture through reaction R4 and R5. The molar Si/Al ratio of the normal and the coarse kaolin powder is 1.12 and 1.17, respectively, which is higher than the theoretical molar Si/Al ratio of kaolinite ($Al_2Si_2O_5(OH)_4$). This is due to the presence of quartz (SiO_2), confirmed by the XRD spectrum of the kaolin powder shown in Figure 1.

As shown in Table 1, the BET surface area of the normal kaolin is 12.70 m^2/g. The BET surface area of the fine and coarse kaolin is similar to that of normal kaolin. However, the BET surface area of mullite is much smaller than that of the parental kaolin, implying a significant sintering process during the mullite preparation process.

The XRD spectra of the normal kaolin, coarse kaolin and the mullite are shown in Figure 1. The XRD spectrum of the fine kaolin is the same as that of the normal kaolin, and thus is not included. The spectra show that kaolinite ($Al_2Si_2O_5(OH)_4$) and quartz (SiO_2) are the main mineral phases in the three kaolin samples. In the mullite sample, mullite ($3Al_2O_3·2SiO_2$) and quartz (SiO_2) are detected as the main mineral phases. No kaolinite was detected in the mullite sample, indicating a complete transformation from kaolinite to mullite during heat treatment.

2.2 Setup

Experiments were conducted in the DTU Entrained Flow Reactor (EFR), as shown in Figure 2, which can simulate the conditions in suspension-fired boilers. The EFR consists of a gas supply system, a liquid/slurry sample feeding system, a gas preheater, a vertical reactor which is electrically

heated by 7 heating elements, a bottom chamber and a particle and a flue gas extraction system. The vertical reactor tube is 2-meter long, and the inner diameter is 79 mm. The reactor can be heated up to 1450 °C. A 0.8 m long preheater is placed above the reactor tube for preheating the secondary gas.

To obtain a high KOH vaporization degree and a good contact of salt vapor to additives, a slurry containing KOH and kaolin was fed into the EFR, instead of feeding solid KOH and kaolin powder into the reactor directly.[74, 75] The slurry was subsequently fed into the reactor, using a peristaltic pump through a water-cooled feeding probe, as shown in Figure 3. During each experiment, the slurry was stirred with a magnetic stirrer to keep it homogeneous.

The slurry also contained ethanol, which combusted in the reactor producing CO_2. Therefore, the feeding rate stability can be indirectly monitored by measuring the CO_2 concentration in the flue gas. Slurry fed into the reactor was atomized, at the outlet of the water-cooled feeding probe by a 30 Nl/min primary air flow, as shown in Figure 3. The atomized slurry droplets were mixed with the preheated secondary air and subsequently evaporated. KOH transferred into gas phase and reacted with solid additives (kaolin or mullite) in the reactor tube. At the outlet of the reactor, the flue gas and the entrained solid samples entered into a water-cooled bottom chamber, where the flue gas was divided into two fractions, with around 50 % going to the sampling probe and subsequently to the solid sampling line, while the remaining 50 % vent to the ventilation, directly. The sampling probe is about 1.5 meters long and is air-cooled, keeping the flue gas temperature at around 300 °C. A 10 Nl/min quench gas was introduced at the inlet of the sampling probe, for quenching the flue gas and the reaction. The quenching gas also helped to prevent the deposition of solid samples on the inner wall of the sampling tube. The entrained large solid particles and aerosols were captured, respectively, by a cyclone (with a cut-off diameter of 2.3 µm) and a metal filter (with a pore size of 0.8 µm) in the

sampling line. The cyclone and filter were both heated to 200 °C, to avoid condensation of water vapor. Each experiment lasted about 60 min, and the solid samples were collected for further analysis.

In order to avoid unexpected air leakage into the EFR, the reactor was operated at a pressure slightly higher (approximately 1.0-3.0 mbar) than the atmospheric pressure, and the possible gas escaping from the reactor was captured by a shell around the reactor and pumped to ventilation.

2.3 Experimental matrix

Two sets of experiments were conducted in the EFR: KOH evaporation experiments and KOH-capture experiments using kaolin of three different particle sizes, and mullite. The experimental conditions are summarized in Table 2, and more detailed information is available in Appendix I of the supplementary material. In the KOH evaporation experiments (experiment series (A) in Table 2), KOH solution was injected into the EFR without solid additives, to study the evaporation and transformation behavior of KOH at high temperature. The concentration of KOH in the flue gas was kept at 500 ppmv. The mass of solid samples collected in the cyclone and filter were weighted to study the vaporization of KOH. Additionally, the collected solid samples were analyzed with XRD to determine the transformation of KOH at high temperatures.

In the KOH-capture experiments (experiment series (B to F) in Table 2), a slurry containing both KOH and kaolin/mullite was injected into the EFR. In all the KOH-capture experiments, the concentration of kaolin in the flue gas was kept constant, while the amount of KOH in the feeding slurry was adjusted. Thereby, the concentration of KOH in the flue gas was changed consequently. The KOH-concentration (K-concentration in Table 2) in the flue gas was changed from 50 ppmv to 1000 ppmv, and the molar ratio of K/(Al+Si) in reactants was changed from 0.048 to 0.961 correspondingly.

9

2.4 Analytical methods

To quantify the amount of potassium captured by kaolin, the reacted solid samples were analyzed with ICP-OES (Inductively Coupled Plasma Atomic Emission Spectroscopy). The concentration of major elements (Al, Ca, Fe, Mg, P, S, K, Si, Na and Ti) was determined according to the Danish Standard of DS/EN 15290 (Solid Biofuels- Determination of Major Elements). The standard DS/EN ISO 16995 (Solid Biofuels- Determination of water soluble Chloride, Sodium and Potassium) was used to determine the concentration of water-soluble K and Cl. The concentration of total potassium and water-soluble potassium of product samples were both analyzed.

Two parameters were defined for quantifying the amount of potassium captured by kaolin: the K-conversion (X_K), and the K-capture level (C_K). X_K is defined as the percentage (%) of input KOH chemically captured by solid additives (kaolin/mullite) forming water-insoluble K-aluminosilicate. C_K is the mass of potassium captured by 1 g of additive (kaolin/mullite) (g K/g additive).

As shown in Figure 4, potassium in the reactants originated both from the salt (KOH) and the additives (kaolin/mullite). The majority of potassium in the reactants was from KOH, which was water-soluble (part A). The remaining potassium was from additives and it was water-insoluble (part D). During the KOH-capture reaction, a part of the water-soluble K reacted with kaolin/mullite forming water-insoluble K-aluminosilicate (part C) while the unreacted KOH remained water-soluble (part B). The K-conversion (X_K), and K-capture level (C_K) were calculated basing on the ICP-OES analysis results of reacted samples as shown in equation 1 and 2.

$$X_K = \frac{C}{A} \times 100\ \%$$

(1)

$$C_K = \frac{n_{KOH} M_K X_K}{m_{ad.}}$$

(2)

In equation 1, C is the amount of water-insoluble potassium formed by the K-capture reaction, and A is the amount of potassium from KOH fed into the reactor, as shown in Figure 4. n_{Ksalt} (mol) is the molar amount of KOH fed into the reactor, M_K is the molar mass of K (g/mol) and $m_{ad.}$ is the mass of solid additives fed into the reactor (g). The details of the method for quantifying K-capture can be found in Appendix II of the supplementary material.

To characterize the mineralogical composition of the reacted solid products, the collected samples were washed with deionized water at room temperature for 24 hours to remove the water-soluble compounds (i.e. the K-salts in the reactant), and then filtered using 0.4 μm membranes. Subsequently, the water-washed solid samples were subjected to X-ray diffractometry (XRD) analysis. The XRD spectra were determined with a Huber diffractometer with characteristic Cu Kα radiation and operation conditions of 40 kV and 40 mA. The wave length was 1.54056 Å. The identification of the main crystalline phase was performed with the JADE 6.0 software package (MDI Livermore, CA) and the diffraction database of PDF2-2004.

2.5 Equilibrium Calculations

To understand the transformation of KOH at high temperature, global equilibrium calculations at the same conditions as shown in experimental series (A) of Table 2 were conducted. To make a comparison of the experimental K-conversion relative to equilibrium, global equilibrium calculations were carried out at the conditions shown in experimental series (B-F) of Table 2. The calculations were performed using the Equilibrium module of the software FactSage 7.0. The databases of FactPS, FToxid, FTsalt and FTpulp were employed for the calculations. Information about the different databases can be found in literature.[76, 77]

3 Results and discussion

3.1 *Evaporation and transformation of KOH in the EFR*

Equilibrium calculations as well as EFR experiments (experimental series (A) in Table 2) were conducted to investigate the evaporation and transformation of KOH at high temperatures. The mass fractions of the collected solid products in cyclone and filter are shown in Figure 5 (A). The results of corresponding equilibrium calculations are shown in Figure 5 (B)**.**

In the EFR sampling system, the large particles were collected in the cyclone, while the aerosols were collected in the filter. When the K-salts were completely vaporized in the reactor and then cooled down in the extraction probe, aerosols would form and all solid products would be collected in the filter. If some of the salt particles generated from evaporation of slurry droplets were not fully vaporized, both aerosols and some larger particles would be present, resulting in some solid material being collected also by the cyclone. The experimental data in Figure 5(A) indicate that a complete vaporization of KOH was obtained at 1100°C. At 800 and 900 °C, the mass fraction of samples collected in the cyclone was 2.0 % and 1.5 % respectively, indicating that a small amount of KOH not evaporated. This is in agreement with the equilibrium calculations (Figure 5(B)), which predict that the majority of KOH appears as vapor at temperatures above 820 °C.

XRD analysis of the solid samples collected from the KOH evaporation experiments showed they consisted of $K_2CO_3 \cdot 1.5H_2O$. During cooling, gaseous or condensed KOH reacts with CO_2 to form K_2CO_3, which then absorbs moisture from the air forming $K_2CO_3 \cdot 1.5H_2O$.

3.2 *Representativeness of solid product samples*

The solid products from the EFR experiments, including samples from the sampling probe, cyclone and filter, were carefully collected. For each experiment the collected solid products corresponded to

about 58 % to 75 % of the theoretical amount solid samples extracted by the probe. The rest were lost, mainly by deposition on the inner wall of the reactor tube.[78]

Therefore, in order to be able to determine the conversion degree of the reaction based on the collected solid product samples, the representativeness of the collected solid product samples were checked. This was done by comparing the molar ratio of K/(Al+Si) in the products with that of the fed reactants. The results based on ICP-OES analysis are shown in Figure 6. The molar ratios of K/(Al+Si) in the collected solid samples are nearly identical to those of the reactants, implying that the solid product samples are representative.

3.3   Evolution of kaolin in the EFR

Slurries of normal kaolin (D_{50} = 5.47 μm) without and with KOH were fed into the EFR at 1300 °C, where the residence time was 1.2 s. XRD and SEM-EDX were utilized to study the mineralogical and morphological evolutions of kaolin during the reaction with KOH. The XRD spectra of the raw kaolin, the dehydroxylated kaolin (i.e. product of kaolin fed into the EFR without KOH), mullite, and the water-washed KOH-captured kaolin samples are compared in Figure 7.

The results show that only mullite and quartz were detected in the dehydroxylated kaolin (Figure 7 c); no kaolinite was detected. This reveals that at 1300 °C, with a residence time of 1.2 s, all kaolinite from raw kaolin has decomposed completely. However, the peaks corresponding to mullite of the dehydroxylated kaolin are obviously weaker compared to the peaks of the mullite powder (Figure 7 b). This shows that not all the decomposed kaolinite was converted to crystalline mullite with some remaining as amorphous species, like metakaolin and amorphous silica.[59] In the water washed KOH-reacted kaolin (Figure 7 a), crystalline kaliophilite ($KAlSiO_4$) was detected, as the reaction product of kaolin and KOH at high temperatures (1300 °C) in the EFR.

13

The SEM images of raw kaolin, the dehydroxylated kaolin and water-washed KOH-reacted kaolin are compared in Figure 8. It is seen that raw kaolin particles are all in a form of an irregular flaky shape, while the dehydroxylated kaolin particles are slightly more spherical but keep the original inner flaky structure. The flaky structure indicates that no significant melting took place at 1300 °C, in agreement with the reported mullite melting point of 1830 °C.[79] For the KOH-reacted kaolin sample, some spherical particles with smooth surface were observed, showing the particles experienced melting in the EFR. Since the kaliophilite ($KAlSiO_4$) detected in the KOH-reacted solid product has a melting point of 1800 °C,[70] it is mostly likely some amorphous products with low melting point were formed as well.

Water-washed KOH-reacted kaolin (Figure 8 (C)) was analyzed with SEM-EDX to get the elemental composition. The result shows that the molar ratio of K:Al:Si is 1:1.18:1.37, i.e., with extra Si compared to the chemical formula of kaliophilite ($KAlSiO_4$). This is attributed to the presence of quartz (SiO_2), which was also detected with the XRD analysis. It could also be due to the formation of some amorphous Si-species, which cannot be detected by XRD analysis.

3.4 Equilibrium calculations

Equilibrium calculations were carried out for the same conditions as in the EFR, but with a wider temperature range from 500 °C to 1800 °C. The influence of both the KOH concentration and thereby the molar K/(Al+Si) ratio in the reactants, and the reaction temperature was studied by the calculations. A summary of the equilibrium calculation results is shown in Table 3. The detailed results of the calculations are shown in Appendix III of the supplementary material.

The results in Table 3 indicate that the main K-aluminosilicate species formed from the reaction between KOH and kaolin varies with the molar ratio of K/(Al+Si) in the input. At 800-1450 °C, with

14

50 ppmv KOH, sanidine ($KAlSi_3O_8$) is the main aluminosilicate product with K:Al:Si = 1:1:3; With 250 ppmv KOH, both sanidine ($KAlSi_3O_8$) and leucite ($KAlSi_2O_6$) are major K-aluminosilicates; while with 500-1000 ppmv KOH, kaliophilite ($KAlSiO_4$) with K:Al:Si = 1:1:1 became the dominating K-aluminosilicate.

3.5 Impact of the potassium concentration

The experimental K-capture level (C_K) and K-conversion (X_K) are compared with the estimations from equilibrium calculations in Figure 9. The KOH-concentration in the flue gas varied from 50 ppmv to 1000 ppmv, while the reaction temperature was kept constant at 1100 °C. The experimental data follows a similar trend but is always slightly lower as compared to the equilibrium prediction. When the KOH concentration increased from 50 ppmv to 500 ppmv, the K-capture level (C_K) by kaolin increased from 0.022 g K/ (g kaolin) to 0.227 g K/ (g kaolin). However, no obvious increase of C_K is observed when the KOH concentration increased further to 750 and 1000 ppmv. This is probably because the active compound in kaolin has been fully converted into K-aluminosilicates, while the increased KOH remained unreacted. The equilibrium constrain can explain the decrease of K-conversion (X_K). X_K decreased slightly from 95.8 % to 84.6 % when the KOH concentration increased from 50 ppmv to 500 ppmv, while X_K decreased sharply when the KOH concentration increased from 500 ppmv to 1000 ppmv as shown in Figure 9 (B).

The XRD spectra of the water-washed KOH-reacted kaolin at 50, 250 and 500 ppmv KOH are compared in Figure 10. The spectra at 750 ppmv and 1000 ppmv were similar to that at 500 ppmv and are not included. The results show that in the 50 ppmv-KOH product, only quartz and mullite were detected as the main crystalline phases. No crystalline K-aluminosilicate was detected in the sample, although sanidine ($KAlSi_3O_8$) was predicted by the equilibrium calculations shown in Table 3. This is

probably because the concentration of K-aluminosilicates is low and/or they remained in an amorphous state, which cannot be detected. The 250 ppmv KOH spectrum shows that leucite ($KAlSi_2O_6$) with a molar ratio of K:Al:Si = 1:1:2 was the main K-aluminosilicate, while kaliophilite ($KAlSiO_4$) with a molar ratio of K:Al:Si = 1:1:1 became the main K-aluminosilicate at 500 ppmv KOH. The XRD analysis results generally agree with the equilibrium calculations shown in Table 3.

3.6 Impact of reaction temperature

The K-capture level (C_K) and K-conversion (X_K) obtained at different reaction temperatures (800-1450 °C) and two different KOH concentrations (50 ppmv and 500 ppmv) were compared with the equilibrium calculation results in Figure 11. Figure 11 (A) and (B) show that, at 500 ppmv KOH, the K-capture level (C_K) increased from 0.166 g K/(g kaolin) to 0.241 g K/(g kaolin) by 43.6 %, when the reaction temperature increased from 800 °C to 1300 °C. The K-conversion (X_K) increased from 62.1 % to 89.1 %, correspondingly. However, when the temperature was increased further to 1450 °C, C_K and X_K decreased to 0.198 g K/(g kaolin) and 74.0 % respectively. This is caused by a change in the equilibrium products with a decreased amount of kaliophilite ($KAlSiO_4$) and an increased amount of leucite ($KAlSi_2O_6$) at high temperatures. At 1300 °C and 1450 °C, the K-capture level (C_K) is close to the equilibrium calculation value. At 1100 °C and below, the K-capture levels (C_K) are below the equilibrium levels, implying the process is kinetic controlled.

Figure 11 (C) and (D) show that at 50 ppmv KOH, the K-capture level (C_K) was predicted to be 0.023 g K/g kaolin, by the equilibrium calculations, and the predicted K-conversion (X_K) was higher than 99.2 % through the whole temperature range. At temperatures above 1100 °C, the experimental C_K and X_K were close to the equilibrium calculations. At 800 °C and 900 °C, the experimental result is

16

slightly lower than the value predicted by the equilibrium calculations. The only K-aluminosilicate predicted by the calculations is sanidine ($KAlSi_3O_8$) with a molar ratio of K:Al:Si = 1:1:3.

The water-washed 500 ppmv KOH-reacted kaolin samples were subjected to XRD analysis, with the spectra shown in Figure 12. It shows that with the temperature increased from 800 to 1450 °C, the peaks of kaliophilite ($KAlSiO_4$) increased significantly, indicating either kaliophilite was generated in larger quantities or that it became more crystalline with the increasing temperature or due to a faster cooling rate in the sampling system. No other crystalline K-aluminosilicate product was detected, although leucite ($KAlSi_2O_6$) was also predicted by the equilibrium calculations. The formation of kaliophilite was also observed in experimental studies by Steenari and her co-workers.[45] Kalsilite ($KAlSiO_4$), a polymorph of kaliophilite was also widely reported in previous studies.[51, 70, 72, 80] At 800 °C and 900 °C, no clear signal of K-aluminosilicate was detected by XRD. This is probably because the formed K-aluminosilicate existed in an amorphous form at lower temperatures. Kaolinite was detected in the 800 and 900 °C solid products, indicating an incomplete dehydroxylation of kaolin at temperatures below 900 °C in the EFR.

3.7 Impact of gas residence time

The impact of gas residence time on the KOH-capture reaction was investigated at 800 °C and 1100 °C. At 800 °C, the gas residence time varied from 1.2 s to 1.9 s, while at 1100 °C, it was changed from 0.7 s to 1.7 s. In all experiments, the KOH-concentration in the flue gas and the molar ratio of K/(Al+Si) in the reactants were kept constant, at 500 ppmv and 0.481, respectively. The experimental results were compared to the equilibrium calculation results in Figure 13.

At 800 °C, as shown in Figure 13 (A), when the gas residence time increased from 1.2 s to 1.9 s, K-capture level (C_K) increases by 25.4 % from 0.166 g K/g kaolin to 0.209 g K/g kaolin. However at

17

1100 °C, when the gas residence time increased from 0.7 s to 1.2 s, C_K increased by 7.6 %, from 0.211 to 0.227 g K/g kaolin. When the gas residence time increased further from 1.2 s to 1.7 s, C_K increased to 0.236 by 4.1 %.

In summary, the KOH-capture reaction by kaolin reached equilibrium at temperatures of 1300 °C and 1450 °C, with a gas residence time of 1.2 s and a kaolin particle size of D_{50} = 5.47 μm. At 1100 °C with a residence time of 1.7 s, the reaction is close to the equilibrium. However, at 800 °C, C_K is obviously further away from the equilibrium even with a longer residence time of 1.9 s, showing that the reaction is more kinetically or diffusion controlled at 800 °C.

3.8 Impact of kaolin particle size

The K-capture level (C_K) of fine kaolin, normal kaolin and coarse kaolin at 800-1450 °C were compared to the equilibrium calculation results in Figure 14. Generally, the results show that at 900-1300 °C fine kaolin and normal kaolin behaved similarly, and C_K did not increase when the D_{50} of kaolin particle size decreased from 5.47 μm to 3.51 μm. For coarse kaolin, C_K is similar as that of normal and fine kaolin at 900 °C. However it became lower than the C_K of normal and fine kaolin at 1100 and 1300 °C. This indicates that the conversion at 1100 and 1300 °C is partly limited by the transport processes, at least for the coarse kaolin. However, at 800 °C the reaction appears to be kinetically limited.

3.9 KOH capture by mullite

The KOH capture level of mullite (D_{50} = 5.90 μm) was compared with that of normal kaolin (D_{50} = 5.47 μm) in Figure 15, at reaction temperatures of 800-1450 °C, gas residence time of 1.2 s and a KOH concentration of 500 ppmv. The EFR experimental results show, that at low temperatures (800 - 1100 °C), C_K of mullite is much lower than that of kaolin. This is probably partly because the BET

surface area of mullite is smaller than that of kaolin (shown in Table 1) and thereby limited the internal KOH transport in the particles. On the other hand, the kinetics of the mullite-KOH reaction is probably slower than that of the kaolin-KOH reaction. At 1300 °C and 1450 °C, C_K of mullite increased significantly, and at 1450 °C, the value is close to that of the normal kaolin powder. This is probably because at high temperatures (1300 and 1450 °C), the KOH-reacted mullite particles are melted, and the KOH diffusion mechanism changed from a slow gas-solid diffusion to a faster gas-liquid diffusion which improved the transport of KOH inside the mullite particles. A similar phenomenon was observed by Zheng et al., when the KCl capture by mullite pellets was studied in a fixed bed reactor.[52]

4   Conclusions

The impact of different parameters, including the potassium concentration in flue gas (molar ratio of K/(Al+Si) in reactants), the reaction temperature, the residence time, the kaolin particle size, as well as the high temperatures phase transformations of kaolin, on the KOH-capture reaction at suspension fired conditions was investigated, by experiments in an entrained flow reactor and by thermodynamic equilibrium calculations.

The K-capture level (C_K) increased significantly when the KOH-concentration increased from 50 to 500 ppmv, corresponding to an increase in the molar K/(Al+Si) ratio from 0.048 to 0.48, whereas no obvious increase was observed when KOH-concentration increased further to 750 ppmv and 1000 ppmv. Leucite ($KAlSi_2O_6$) was formed at 250 ppmv KOH (K/(Al+Si) = 0.240), and kaliophilite ($KAlSiO_4$) was the dominant K-aluminosilicate at 500 ppmv KOH and above (K/(Al+Si) ≥ 0.481).

A nearly full conversion of kaolin (D_{50} = 5.47 μm) was obtained without kinetic or transport limitations at temperatures above 1100 °C and the applied conditions (residence time of 1.2 s, and a

19

KOH concentration of 500 ppmv). However, at 800 and 900 °C, the experimental data were considerably lower than the equilibrium predictions, and the K-capture level increased significantly when residence time increased, implying the reaction is probably kinetically controlled. The optimal temperature window for injecting kaolin for K-capture at suspension-fired conditions is 1100-1300 °C. At 1100 °C or above, crystalline kaliophilite ($KAlSiO_4$) was detected by XRD analysis, while at 800 and 900 °C, amorphous K-aluminosilicate was formed.

Fine kaolin powder (D_{50} = 3.51 μm) and normal kaolin powder (D_{50} = 5.47 μm) behaved similarly in terms of K-capture level (C_K), while coarse kaolin (D_{50} = 13.48 μm) showed a considerably smaller K-capture level at 1100 and 1300 °C. This is probably because KOH diffusion into the kaolin particles became a limiting factor for the coarse kaolin at 1100 °C and above. At 900 °C, where the difference was smaller, the reaction is more kinetically controlled and the additive particle size did not influence the reaction significantly with the applied particle sizes.

Mullite captured KOH less effectively compared to kaolin at temperatures below 1100 °C. However C_K of mullite increased significantly at 1300 °C and 1450 °C. At 1450 °C, the K-capture level of mullite is comparable to that of kaolin.

5 Acknowledgements

Supporting Information. Appendix I of the supporting information: More detailed experimental conditions about the EFR experiments; Appendix II of the supporting information: The details of the quantification method of K-capture level (C_K) and K-conversion (X_K); Appendix III of the supporting

information: Complete results of the equilibrium calculations of KOH capture by normal kaolin (D_{50} = 5.47 µm).

6   References

(1) Hupa, M. *Energy Fuels* **2012**, 26, 4-14.

(2) Wu, H.; Glarborg, P.; Frandsen, F. J.; Dam-Johansen, K.; Jensen, P. A. *Energy Fuels* **2011**, 25, 2862-2873.

(3) Frandsen, F. J. Ash Formation , Deposition and Corrosion When Utilizing Straw for Heat and Power Production. Doctoral Thesis, Technical University of Denmark, 2011.

(4) Andersen, K. H.; Frandsen, F. J.; Hansen, P. F. B.; Wieck-Hansen, K.; Rasmussen, I.; Overgaard, P.; Dam-Johansen, K. *Energy Fuels* **2000**, 14, 765-780.

(5) Bashir, M. S.; Jensen, P. A.; Frandsen, F. J.; Wedel, S.; Dam-johansen, K.; Wadenba, J.; Pedersen, S. T. *Energy Fuels* **2012**.

(6) Hansen, L. A.; Nielsen, H. P.; Frandsen, F. J.; Dam-Johansen, K.; Hørlyck, S.; Karlsson, A. *Fuel Process. Technol.* **2000**, 64, 189-209.

(7) Wang, G.; Shen, L.; Sheng, C. *Energy Fuels* **2012**, 26, 102-111.

(8) Gao, X.; Yani, S.; Wu, H. *Energy Fuels* **2015**, 29, 5171-5175.

(9) Niu, Y.; Zhu, Y.; Tan, H.; Hui, S.; Jing, Z.; Xu, W. *Fuel Process. Technol.* **2014**, 128, 499-508.

(10) Skrifvars, B.-J.; Laurén, T.; Hupa, M.; Korbee, R.; Ljung, P. *Fuel* **2004**, 83, 1371-1379.

(11) Wang, Q.; Yao, H.; Yu, D.; Dai, L.; Xu, M. *Energy Fuels* **2007**, 21, 513-516.

(12) Laxminarayan, Y.; Jensen, P. A.; Wu, H.; Frandsen, F. J.; Sander, B.; Glarborg, P. *Energy Fuels* **2017**, 31, 8733-8741.

(13) Kling, A.; Andersson, C.; Myringer, A.; Eskilsson, D.; Jaras, S. *Appl. Catal., B: Environ.* **2007**, 69, 240-251.

(14) Zheng, Y.; Jensen, A. D.; Johnsson, J. E. *Appl. Catal., B: Environ.* **2005**, 60, 253-264.

(15) Zheng, Y.; Jensen, A. D.; Johnsson, J. E.; Thøgersen, J. R. *Appl. Catal., B: Environ.* **2008**, 83, 186-194.

(16) Zheng, Y.; Jensen, A. D.; Johnsson, J. E. *Ind. Eng. Chem. Res.* **2004**, 43, 941-947.

(17) Kling, Å.; Andersson, C.; Myringer, Å.; Eskilsson, D.; Järås, S. G. *Appl. Catal., B: Environ.* **2007**, 69, 240-251.

(18) Castellino, F.; Jensen, A. D.; Johnsson, J. E.; Fehrmann, R. *Appl. Catal., B: Environ.* **2009**, 86, 206-215.

(19) Dayton, D. C.; French, R. J.; Milne, T. A. *Energy Fuels* **1995**, 9, 855-865.

(20) Knudsen, J. N.; Jensen, P. A.; Dam-Johansen, K. *Energy Fuels* **2004**, 18, 1385-1399.

(21) Frandsen, F. J. *Fuel* **2005**, 84, 1277-1294.

(22) Nielsen, H. P.; Frandsen, F. J.; Dam-Johansen, K. *Energy Fuels* **1999**, 13, 1114-1121.

(23) Tobiasen, L.; Skytte, R.; Pedersen, L. S.; Pedersen, S. T.; Lindberg, M. A. *Fuel Process. Technol.* **2007**, 88, 1108-1117.

(24) Kassman, H.; Pettersson, J.; Steenari, B.-M.; Åmand, L.-E. *Fuel Process. Technol.* **2013**, 105, 170-180.

(25) Davidsson, K. O.; Åmand, L. E.; Steenari, B. M.; Elled, A. L.; Eskilsson, D.; Leckner, B. *Chem. Eng. Sci.* **2008**, 63, 5314-5329.

(26) De Fusco, L.; Boucquey, A.; Blondeau, J.; Jeanmart, H.; Contino, F. *Fuel* **2016**, 170, 16-26.

(27) Wang, L.; Skjevrak, G.; Hustad, J. E.; Grønli, M.; Skreiberg, Ø. *Energy Procedia* **2012**.

(28) Kyi, S.; Chadwick, B. L. *Fuel* **1999**, 78, 845-855.

(29) Damoe, A. J.; Wu, H.; Frandsen, F. J.; Glarborg, P.; Sander, B. *Energy Fuels* **2014**, 28, 3217-3223.

(30) Boström, D.; Grimm, A.; Boman, C.; Björnbom, E.; Öhman, M. *Energy Fuels* **2009**, 23, 5184-5190.

(31) Sami, M.; Annamalai, K.; Wooldridge, M. *Prog. Energy Combust. Sci.* **2001**, 27, 171-214.

(32) Wu, H.; Glarborg, P.; Frandsen, F. J.; Dam-Johansen, K.; Jensen, P. A.; Sander, B. *Fuel Process. Technol.* **2013**, 105, 212-221.

(33) Wu, H.; Glarborg, P.; Frandsen, F. J.; Dam-Johansen, K.; Jensen, P. A.; Sander, B. *Fuel* **2011**, 90, 1980-1991.

(34) Savolainen, K. *Appl. Energy* **2003**, 74, 369-381.

(35) Wu, H. Co-combustion of Fossil Fuels and Waste. Ph.D. Thesis, Technical University of Denmark, 2011.

(36) Yin, C.; Rosendahl, L. A.; Kær, S. K. *Prog. Energy Combust. Sci.* **2008**, 34, 725-754.

(37) Jensen, P. A.; Sander, B.; Dam-Johansen, K. *Biomass Bioenergy* **2001**, 20, 431-446.

(38) Llorente, M. J. F.; Arocas, P. D.; Nebot, L. G.; García, J. E. C. *Fuel* **2008**, 87, 2651-2658.

(39) Si, J.; Liu, X.; Xu, M.; Sheng, L.; Zhou, Z.; Wang, C.; Zhang, Y.; Seo, Y.-C. *Appl. Energy* **2014**, 114, 434-444.

(40) Wu, H.; Bashir, M. S.; Jensen, P. A.; Sander, B.; Glarborg, P. *Fuel* **2013**, 113, 632-643.

(41) Wu, H.; Pedersen, M. N.; Jespersen, J. B.; Aho, M.; Roppo, J.; Frandsen, F. J.; Glarborg, P. *Energy Fuels* **2014**, 28, 199-207.

(42) Aho, M.; Vainikka, P.; Taipale, R.; Yrjas, P. *Fuel* **2008**, 87, 647-654.

(43) Wibberley, L. J.; Wall, T. F. *Fuel* **1982**, 61, 93-99.

(44) Bäfver, L. S.; Rönnbäck, M.; Leckner, B.; Claesson, F.; Tullin, C. *Fuel Process. Technol.* **2009**, 90, 353-359.

(45) Steenari, B. M.; Lindqvist, O. *Biomass Bioenergy* **1998**, 14, 67-76.

(46) Wang, L.; Skreiberg, Ø.; Becidan, M. *Appl. Therm. Eng.* **2014**, 70, 1262-1269.

(47) Aho, M.; Paakkinen, K.; Taipale, R. *Fuel* **2013**, 103, 562-569.

(48) Wang, L.; Hustad, J. E.; Skreiberg, Ø.; Skjevrak, G.; Grønli, M. *Energy Procedia* **2012**, 20, 20-29.

(49) Wang, L.; Skjevrak, G.; Hustad, J. E.; Skreiberg, Ø. *Energy Fuels* **2014**, 28, 208-218.

(50) Turn, S. Q.; Kinoshita, C. M.; Ishimura, D. M.; Zhou, J.; Hiraki, T. T.; Masutani, S. M. *J. Inst. Energy* **1999**, 71, 163-177.

(51) Tran, K.-Q.; Iisa, K.; Steenari, B.-M.; Lindqvist, O. *Fuel* **2005**, 84, 169-175.

(52) Zheng, Y.; Jensen, P. A.; Jensen, A. D. *Fuel* **2008**, 87, 3304-3312.

(53) De Fusco, L.; Defoort, F.; Rajczyk, R.; Jeanmart, H.; Blondeau, J.; Contino, F. *Energy Fuels* **2016**, 30, 8304-8315.

(54) Öhman, M.; Boström, D.; Nordin, A.; Hedman, H. *Energy Fuels* **2004**, 18, 1370-1376.

(55) Aho, M.; Silvennoinen, J. *Fuel* **2004**, 83, 1299-1305.

(56) Ahmaruzzaman, M. *Prog. Energy Combust. Sci.* **2010**, 36, 327-363.

(57) Chen, Y.; Wang, G.; Sheng, C. *Energy Fuels* **2013**.

(58) Aho, M. *Fuel* **2001**, 80, 1943-1951.

(59) Chen, C. Y.; Lan, G. S.; Tuan, W. H. *Ceram. Int.* **2000**, 26, 715-720.

(60) Shadman, F.; Punjak, W. A. *Thermochim. Acta* **1988**, 131, 141-152.

(61) Uberoi, M.; Punjak, W. A.; Shadman, F. *Prog. Energy Combust. Sci.* **1990**, 16, 205-211.

(62) Escobar, I.; Oleschko, H.; Wolf, K.-J.; Müller, M. *Powder Technol.* **2008**, 180, 51-56.

(63) Mwabe, P. O.; Wendt, J. O. L. Mechanisms governing trace sodium capture by kaolinite in a downflow combustor, In *26th Symposium on Combustion*, Napoli Italy, 1996.

(64) Vuthaluru, H. B.; Vleeskens, J. M.; Wall, T. F. *Fuel Process. Technol.* **1998**, 55, 161-173.

(65) Li, M.; Zhang, Z.; Wu, X.; Fan, J. *Energy Fuels* **2016**, 30, 7763-7769.

(66) Chen, Y.; Xu, Y.; Sheng, C. *Proc. CSEE* **2016**, 36, 4396-4410.

(67) Niu, Y.; Tan, H.; Hui, S. e. *Prog. Energy Combust. Sci.* **2016**, 52, 1-61.

(68) Wei, X.; Schnell, U.; Hein, K. *Fuel* **2005**, 84, 841-848.

(69) Michelsen, H. P. Deposition and high-temperature corrosion in biomass-fired boilers. Ph.D. Thesis, Technical University of Denmark, 1998.

(70) Mwabe, P. O. Mechanisms governing alkali metal capture by kaolinite in a downflow combustor. Ph.D. Thesis, The University of Arizona, 1993.

(71) Gale, T. K.; Wendt, J. O. L. *Combust. Flame* **2002**, 131, 299-307.

(72) Tran, K.-Q.; Iisa, K.; Hagström, M.; Steenari, B.-M.; Lindqvist, O.; Pettersson, J. B. C. *Fuel* **2004**, 83, 807-812.

(73) Tran, Q. K.; Steenari, B.-M.; Iisa, K.; Lindqvist, O. *Energy Fuels* **2004**, 18, 1870-1876.

(74) Zheng, Y.; Jensen, P. A.; Jensen, A. D. *Potassium capture by kaolin and fly ash powder in an entrained flow reactor*, Technical University of Denmark: Denmark, 2008, 1-51.

(75) Iisa, K.; Lu, Y.; Salmenoja, K. *Energy Fuels* **1999**, 13, 1184-1190.

(76) Bale, C. W.; Chartrand, P.; Degterov, S. A.; Eriksson, G.; Hack, K.; Ben Mahfoud, R.; Melançon, J.; Pelton, A. D.; Petersen, S. *Calphad.* **2002**, 26, 189-228.

(77) Bale, C. W.; Bélisle, E.; Chartrand, P.; Decterov, S. A.; Eriksson, G.; Hack, K.; Jung, I. H.; Kang, Y. B.; Melançon, J.; Pelton, A. D.; Robelin, C.; Petersen, S. *Calphad.* **2009**, 33, 295-311.

(78) Theis, M.; Mueller, C.; Skrifvars, B.-J.; Hupa, M.; Tran, H. *Fuel* **2006**, 85, 1970-1978.

(79) Schneider, H.; Schreuer, J.; Hildmann, B. *J. Eur. Ceram. Soc.* **2008**, 28, 329-344.

(80) Punjak, W. A.; Shadman, F. *Energy Fuels* **1988**, 2, 702-708.

FIGURES
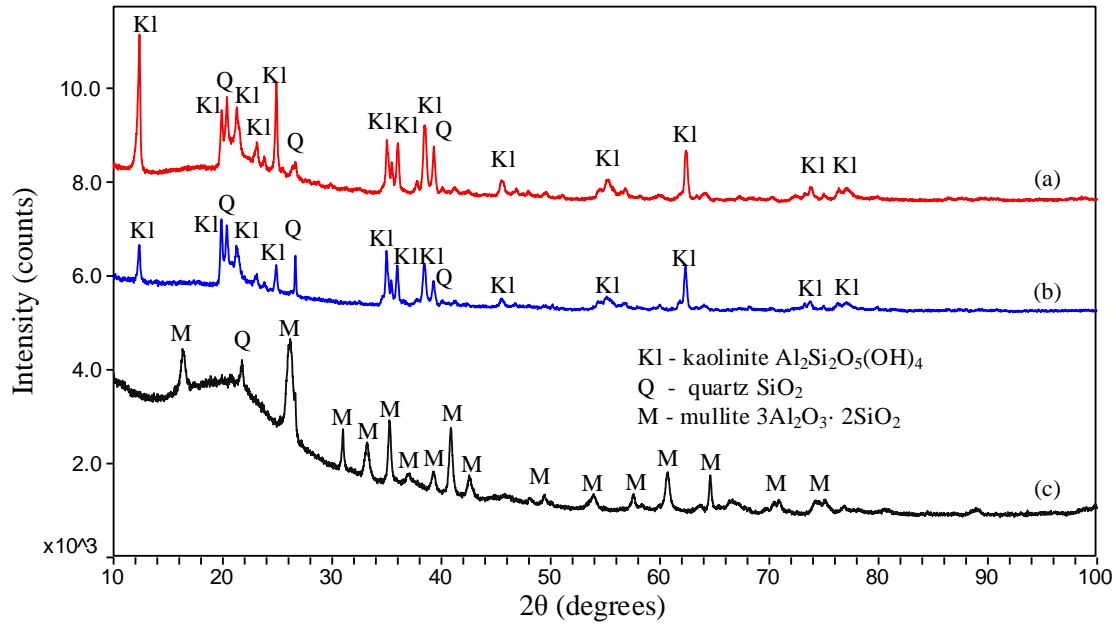
Figure 1. XRD spectra of the kaolin and mullite: normal kaolin with D_{50} = 5.47 μm (a); coarse kaolin with D_{50} = 13.48 μm (b); mullite (c).
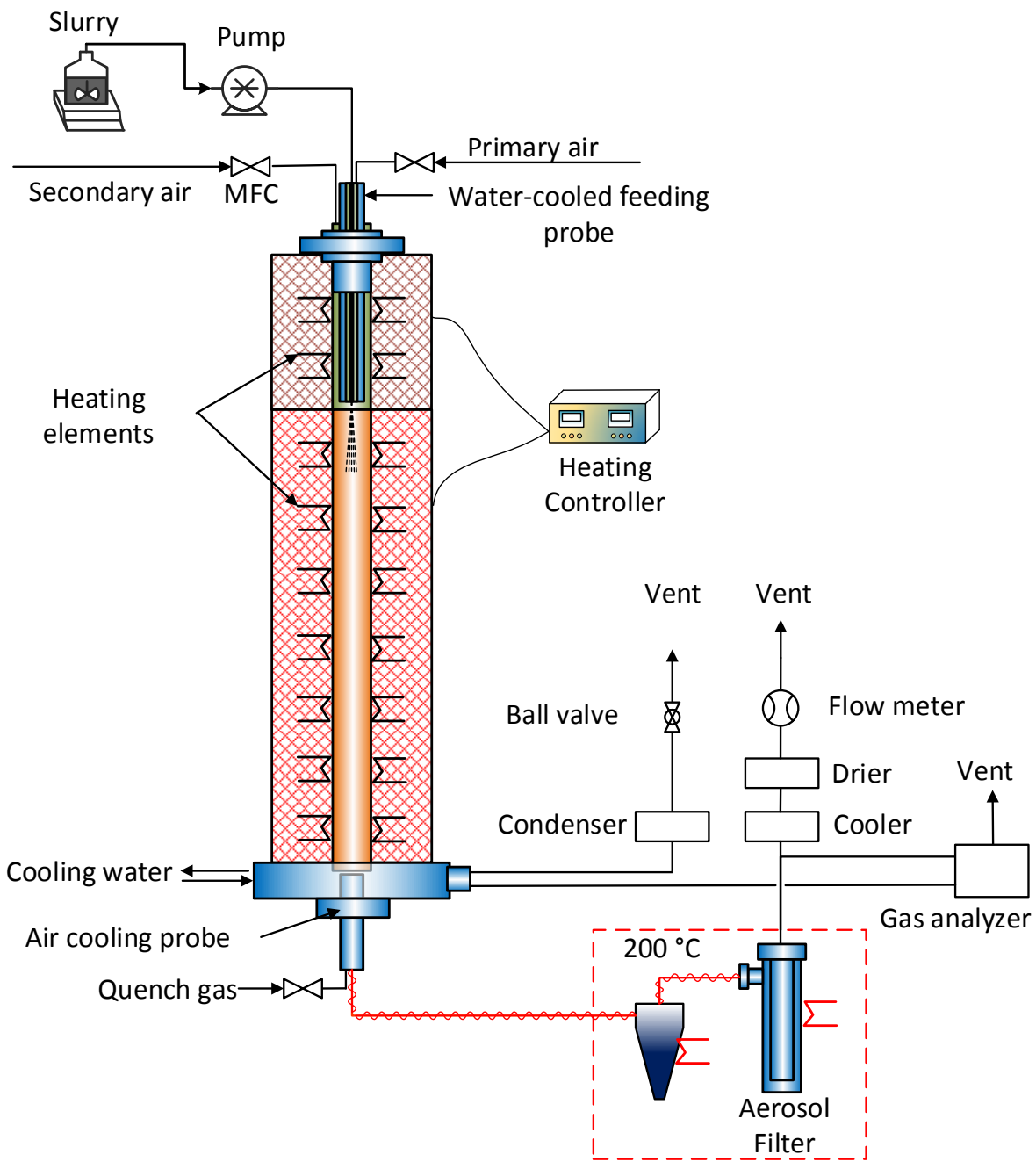
Figure 2. Schematic of the Entrained Flow Reactor (EFR).
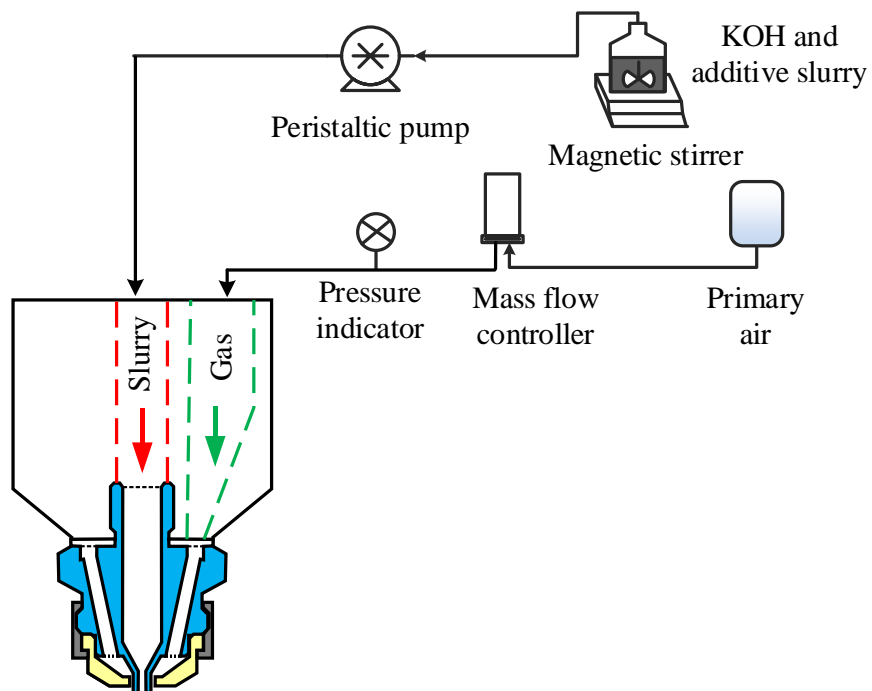
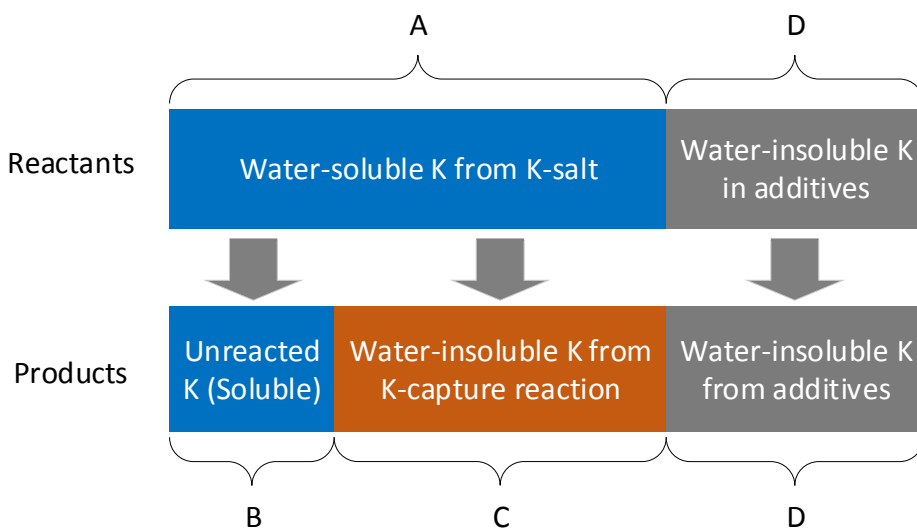Figure 3. Slurry feeding and atomizing system of the DTU Entrained Flow Reactor (EFR).

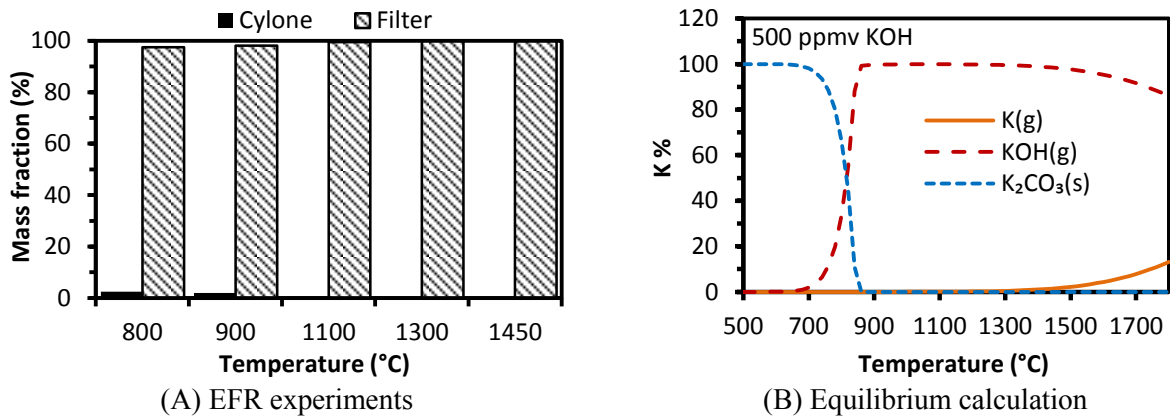Figure 4. Potassium transformations in the K-capture reaction.

Figure 5. Mass distribution of solid samples collected in cyclone and filter from KOH evaporation experiments (A); Equilibrium calculation results of KOH evaporation under conditions of experimental series A of Table 2 (B).
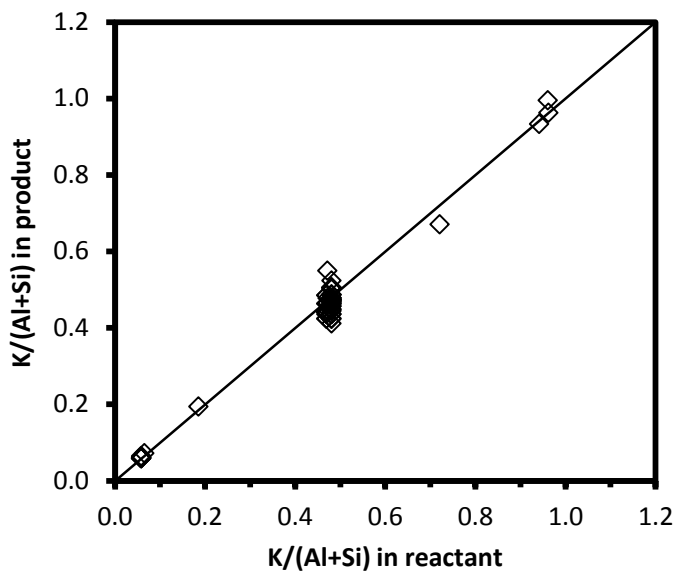
Figure 6. Comparison of K/(Al+Si) in collected solid products and that of fed reactants.
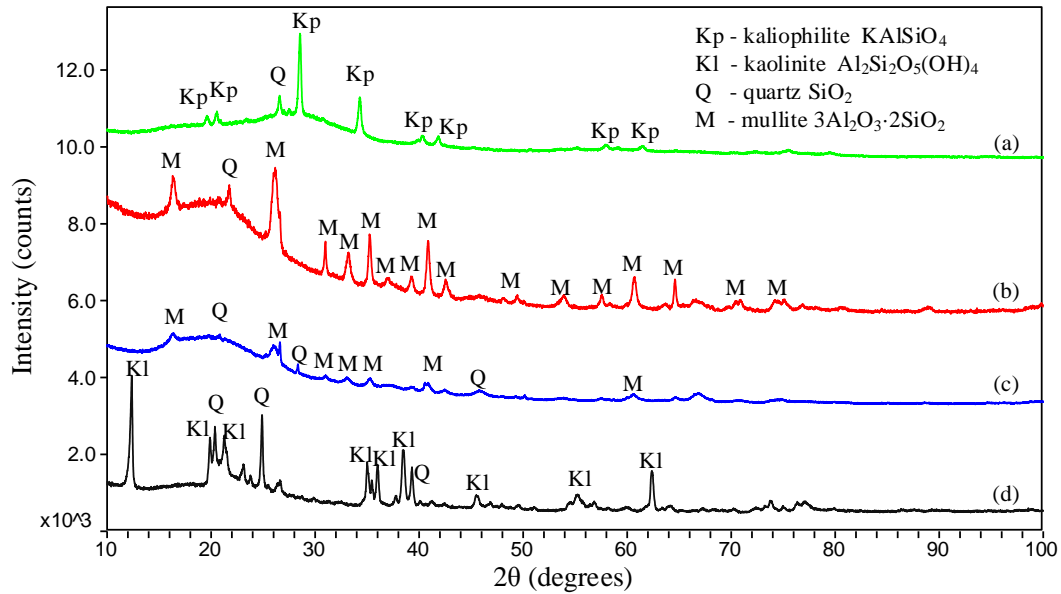
Figure 7. XRD spectra of water-washed kaolin after reaction with 500 ppmv KOH. KOH-reacted kaolin (a); mullite (1100 °C, 24 hours) (b); dehydroxylated kaolin (c); and raw kaolin (d). For sample (a) and (c), reaction temperature in the EFR was 1300 °C, and the gas residence time was 1.2 s.
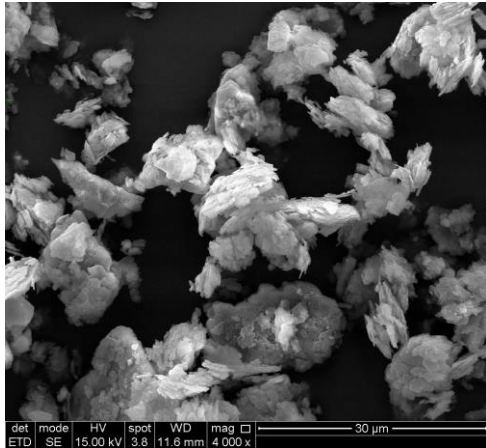
(A) Raw kaolin
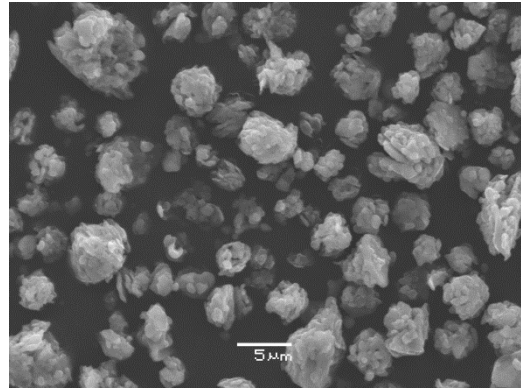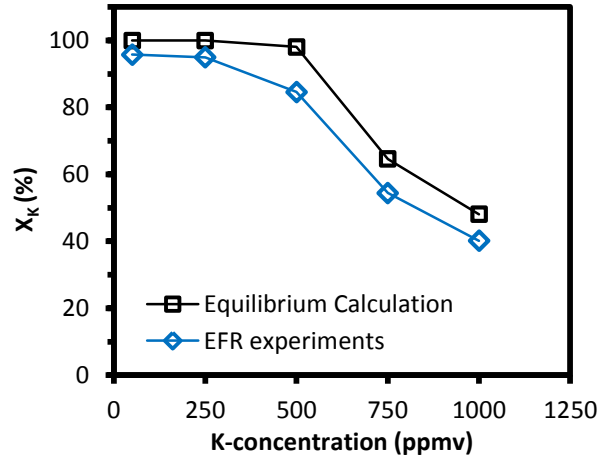

(B) Dehydroxylated kaolin
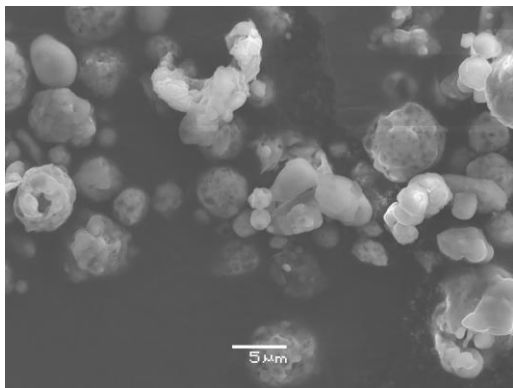
(C) KOH-reacted kaolin

Figure 8. SEM images of raw kaolin (A); dehydroxylated kaolin (without KOH fed at 1300 °C, residence time was 1.2 s) (B); and water-washed KOH-reacted kaolin (C) (500 ppmv KOH by kaolin at 1300 °C, residence time was 1.2 s, K/(Al+Si) in reactant is 0.481).
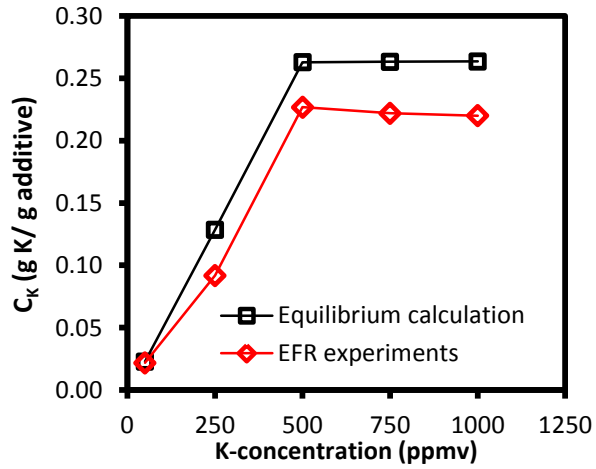
(A) K-capture level (C_K) (B) K-conversion (X_K)

Figure 9. K-capture level (C_K) and K-conversion (X_K) of KOH-capture by normal kaolin (D_{50} = 5.47 μm) at different KOH concentrations from 50 ppmv to 1000 ppmv (molar K/(Al+Si) ratio in reactants varied from 0.048 to 0.961). Reaction temperature was 1100 °C and gas residence time was 1.2 s.
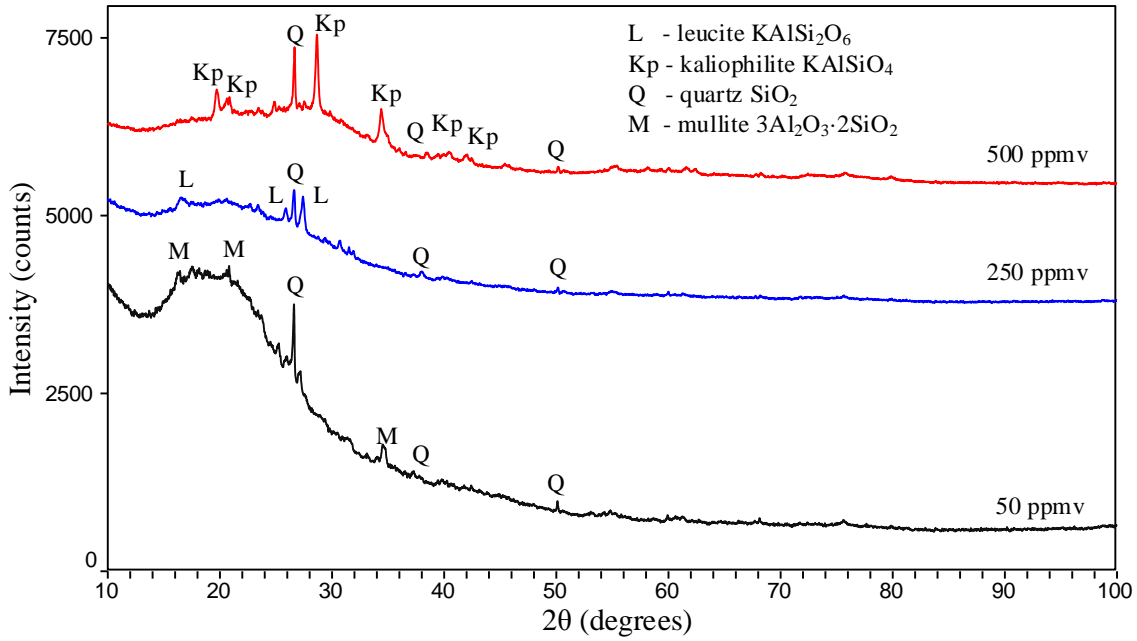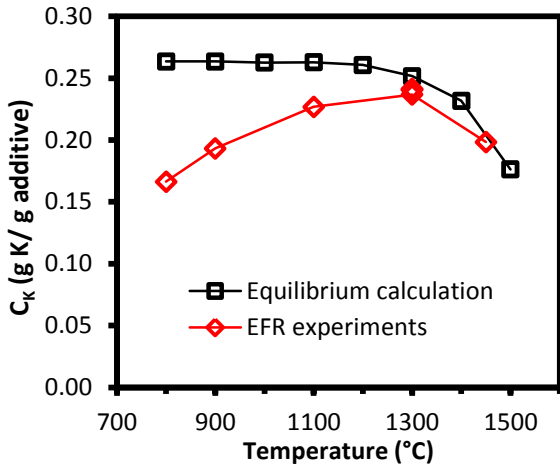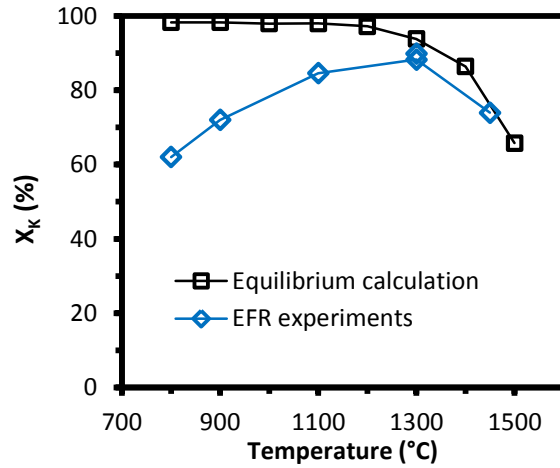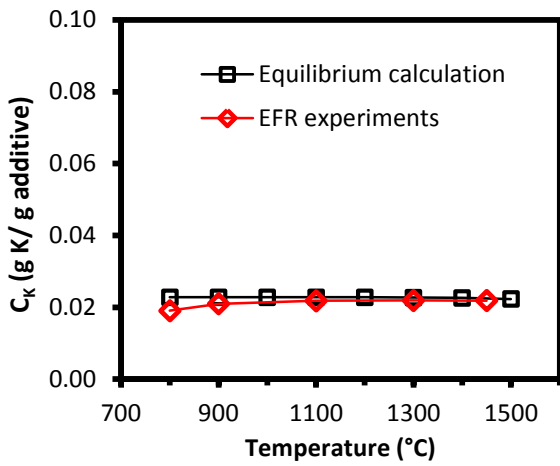
Figure 10. XRD spectra of water-washed KOH-reacted kaolin at 50, 250 and 500 ppmv KOH. The reaction temperature was 1100 °C, the molar ratio of K/(Al+Si) was 0.048, 0.240 and 0.481 and the gas residence time was 1.2 s.
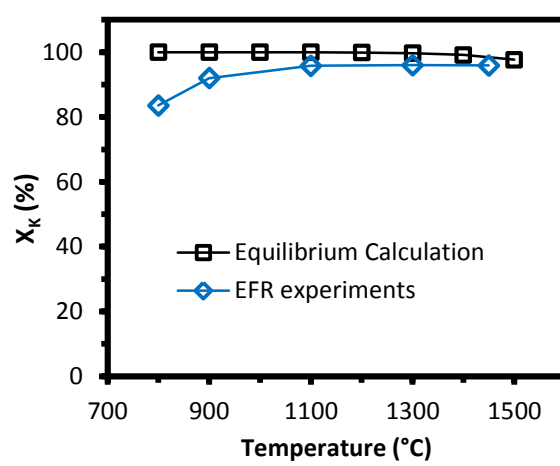
Figure 11. K-capture level (C_K) and K-conversion (X_K) of KOH capture by normal kaolin (D_{50} = 5.47 μm) at temperatures from 800 to 1450 °C. KOH-concentration was 500 ppmv, and molar K/(Al+Si) ratio was 0.481 in (A) and (B); KOH-concentration was 50 ppmv, molar K/(Al+Si) ratio was 0.048 in (C) and (D). Gas residence time was 1.2 s for all experiments, and equilibrium calculation results included for comparison.
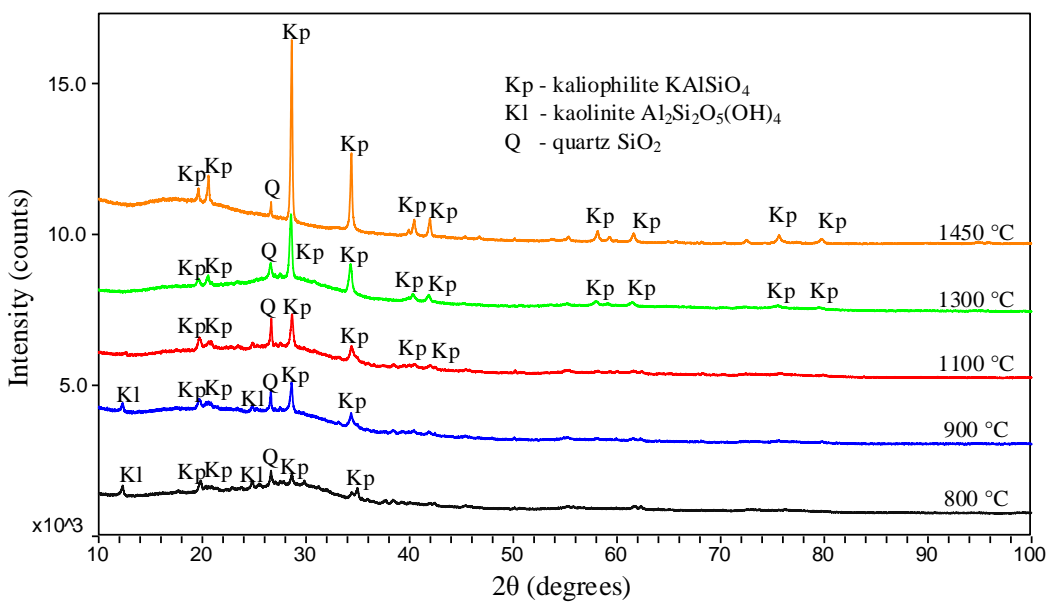
Figure 12. XRD spectra of water-washed solid samples from the experiments of KOH capture by normal kaolin (D_{50} = 5.47 μm) at different reaction temperatures, from 800 °C to 1450 °C. KOH concentration was 500 ppmv, (K/(Al+Si) = 0.481) and the gas residence time was 1.2 s.
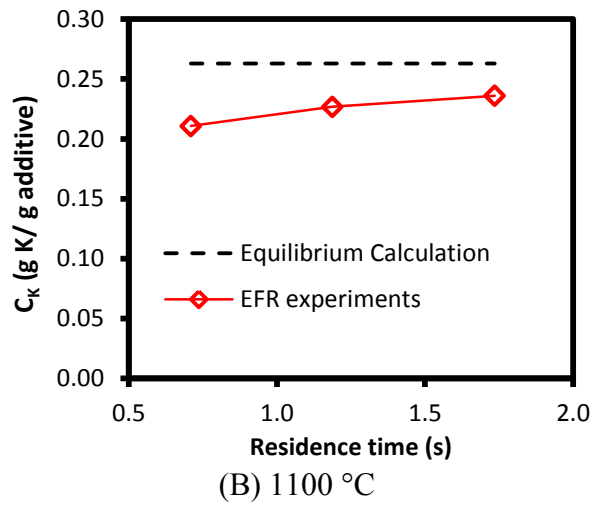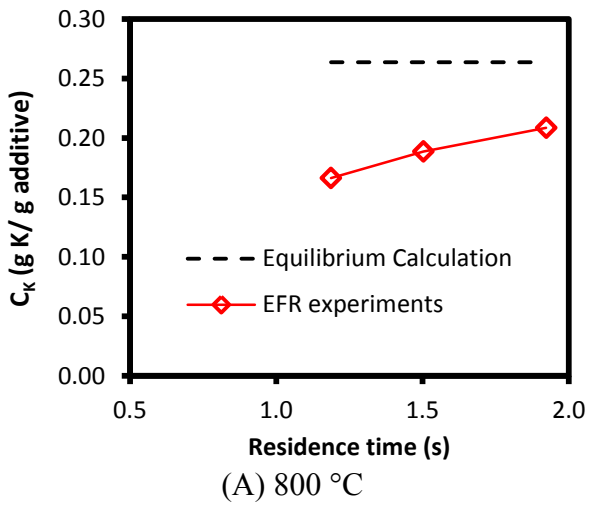
Figure 13. K-capture level (C_K) of KOH capture by the normal kaolin (D_{50} = 5.47 μm) at different gas residence times. Reaction temperature was 800 °C (A) and 1100 °C (B) respectively, and the KOH-concentration was 500 ppmv (K/(Al+Si)= 0.481). Equilibrium calculation results are included for comparison.
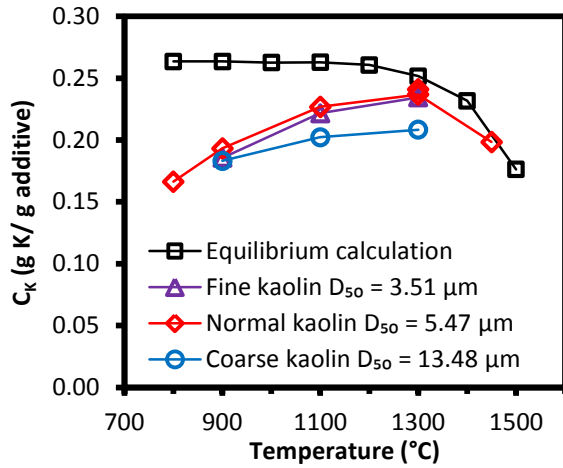
Figure 14. K-capture level (C_K) of KOH capture by kaolin of different particle size: fine kaolin (D_{50} = 3.51 μm), normal kaolin (D_{50} = 5.47 μm) and coarse kaolin (D_{50} = 13.48 μm). KOH concentration was 500 ppmv (molar ratio of K/(Al+Si) in reactant was 0.481), and gas residence time was 1.2 s. Equilibrium calculations are included for comparison.

Figure 15. Comparison of K-capture level (C_K) of KOH capture by kaolin and mullite. Reaction temperature changed from 800 °C to 1450 °C. KOH concentration was 500 ppmv (K/(Al+Si) =

0.481), and gas residence time was 1.2 s. Equilibrium calculation results are included for comparison.
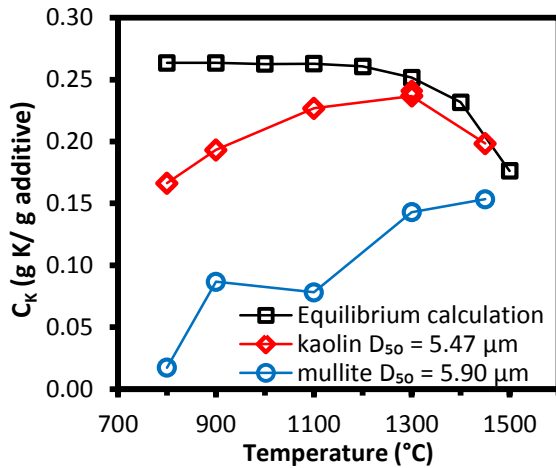
TABLES

Table 1. Characteristics of the solid additives.

	Fine kaolin	Normal kaolin	Coarse kaolin	Mullite
O (wt.%, dry)	56.9	56.9	55.88	51.30
S (wt.%, dry)	0.02	0.02	0.03	0.02
Si (wt.%, dry)	22.0	22.0	23.0	24.8
Al (wt.%, dry)	19.0	19.0	19.0	21.4
Fe (wt.%, dry)	0.47	0.47	0.46	0.53
Ca (wt.%, dry)	0.1	0.1	0.1	0.11
Mg (wt.%, dry)	0.14	0.14	0.12	0.16
Na (wt.%, dry)	0.1	0.1	0.1	0.1
K (wt.%, dry)	1.1	1.1	1.2	1.2
Ti (wt.%, dry)	0.02	0.02	0.01	0.02
P (wt.%, dry)	0.05	0.05	0.05	0.06
Cl (wt.%, dry)	0.1	0.1	0.05	0.11
D_{50} (µm)	3.51	5.47	13.48	5.90
BET surface area(m^2/g)	13.02	12.70	11.83	5.30

Table 2. Conditions of experiments in the Entrained Flow Reactor (EFR).

Experimental series	Additives	Temp./°C	Gas residence time/s	K-concentration /ppmv	K/(Al+Si)
(A) KOH evaporation experiments	No additive	800 900 1100 1300 1450	1.2	500	No Al, Si
(B) KOH-capture by kaolin (impact of **K-concentration**)	normal kaolin (D_{50} = 5.47 μm)	1100	1.2	50 250 500 750 1000	0.048 0.240 0.481 0.721 0.961
(C) KOH-capture by kaolin (impact of **temperature**)	normal kaolin (D_{50} = 5.47 μm)	800 900 1100 1300* 1450	1.2	50, 500	0.048, 0.481
(D) KOH-capture by kaolin (impact of **residence time**)	normal kaolin (D_{50} = 5.47 μm)	800, 1100	0.7 1.2 1.5 1.9	500	0.481
(E) KOH-capture by kaolin (impact of **kaolin particle size**)	fine kaolin (D_{50} = 3.51 μm)	900, 1100, 1300	1.2	500	0.481
	normal kaolin (D_{50} = 5.47 μm)	800, 900, 1100, 1300*, 1450			
	coarse kaolin (D_{50} = 13.48 μm)	900, 1100, 1300			
(F) KOH-capture by **mullite**	Mullite (D_{50} = 5.90 μm)	800, 900, 1100, 1300, 1450	1.2	500	0.471

Note: *Experiments were repeated.

Table 3. Summary of the equilibrium calculation results of KOH capture by kaolin.

Input conditions	Temp. /°C	K-species appearing	Al-con.	Si-con.	K-con.	K-capture/(g K/g kaolin)
50 ppmv KOH, K/(Al+Si) = 0.048	800	100 % $KAlSi_3O_8$	9 %	23 %	100 %	0.023
	900	100 % $KAlSi_3O_8$	9 %	23 %	100 %	0.023
	1100	100 % $KAlSi_3O_8$	9 %	23 %	100 %	0.023
	1300	100 % $KAlSi_3O_8$	9 %	23 %	100 %	0.023
	1450	99 % $KAlSi_3O_8$ + 1 % KOH	9 %	23 %	99 %	0.022
250 ppmv KOH, K/(Al+Si) = 0.240	800	25 % $KAlSi_3O_8$ + 75 % $KAlSi_2O_6$	49 %	98 %	100 %	0.129
	900	25 % $KAlSi_3O_8$ + 75 % $KAlSi_2O_6$	49 %	98 %	100 %	0.129
	1100	24 % $KAlSi_3O_8$ + 76 % $KAlSi_2O_6$	49 %	97 %	100 %	0.129
	1300	20 % $KAlSi_3O_8$ + 80 % $KAlSi_2O_6$	49 %	96 %	100 %	0.128
	1450	22 % $KAlSi_3O_8$ + 77 % $KAlSi_2O_6$	49 %	96 %	99 %	0.128
500 ppmv KOH, K/(Al+Si) = 0.481	800	92 % $KAlSiO_4$ + 6 % $KAlSi_2O_6$	100 %	98 %	98 %	0.264
	900	91 % $KAlSiO_4$ + 7 % $KAlSi_2O_6$ +1 % KOH	100 %	99 %	98 %	0.264
	1100	91 % $KAlSiO_4$ + 7 % $KAlSi_2O_6$ +2 % KOH	100 %	99 %	98 %	0.263
	1300	82 % $KAlSiO_4$ + 12 % $KAlSi_2O_6$ + 6 % KOH	95 %	100 %	94 %	0.252
	1450	50 % $KAlSiO_4$ + 28 % $KAlSi_2O_6$ + 21 % KOH	79 %	100 %	78 %	0.209
750 ppmv KOH, K/(Al+Si) = 0.721	800	57 % $KAlSiO_4$ + 8 % $KAlO_2$ + 31 % K_2SiO_3 + 3 % KOH	88 %	78 %	57 %	0.231
	900	63 % $KAlSiO_4$ + 1 % $KAlO_2$ + 18 % K_2SiO_3 + 16 % KOH	98 %	87 %	63 %	0.258
	1100	65 % $KAlSiO_4$ + 8 % $K_2Si_2O_5$ + 27 % KOH	100 %	89 %	65 %	0.263
	1300	57 % $KAlSiO_4$ + 8 % $KAlSi_2O_6$ + 35 % KOH	100 %	100 %	65 %	0.263
	1450	57 % $KAlSiO_4$ + 8 % $KAlSi_2O_6$ + 35 % KOH	100 %	100 %	65 %	0.263
1000 ppmv KOH, K/(Al+Si) = 0.961	800	29 % $KAlSiO_4$ + 19 % $KAlO_2$ + 49 % K_2SiO_3 + 3 % KOH	61 %	55 %	29 %	0.161
	900	35 % $KAlSiO_4$ + 13 % $KAlO_2$ + 38 % K_2SiO_3 + 14 % KOH	73 %	65 %	35 %	0.191
	1100	48 % $KAlSiO_4$ + 11 % K_2SiO_3 + 41 % KOH	100 %	89 %	48 %	0.264
	1300	43 % $KAlSiO_4$ + 6 % $KAlSi_2O_6$ + 52 % KOH	100 %	100 %	48 %	0.264
	1450	43 % $KAlSiO_4$ + 6 % $KAlSi_2O_6$ + 51 % KOH + 1 % K	100 %	100 %	48 %	0.264